Wind and Structures, *Vol. 27, No. 5 (2018) 347-356*
DOI: https://doi.org/10.12989/was.2018.27.5.347

Evaluation of stress distribution with wind speed in a greenhouse structure

Deog-jae Hur[*1], Jung-Hun Noh[1a], Hyun ju Lee[1b] and Hyoung woon Song[2c]

[1]Research & Business Corporation Center, Institute for Advanced Engineering, 175-28,Goan-ro, 51 beon-gil, Beagam-myeon, Cheoin-gu,Yongin-si, Gyeonggi-do, Republic of Korea
[2]Plant Engineering Division, Institute for Advanced Engineering, 175-28,Goan-ro, 51 beon-gil, Beagam-myeon, Cheoin-gu,Yongin-si, Gyeonggi-do, Republic of Korea

(Received October 11, 2017, Revised May 9, 2018, Accepted May 30, 2018)

Abstract. In this paper, stress distribution for a structurally stable greenhouse is considered in the present paper with subsequent investigation into the detailed stress distribution contour with the variation of self-weight and wind pressure level designation method under wind velocity of less than 30 m/sec. For reliable analysis, wind pressure coefficients of a single greenhouse unit were modeled and compared with experiment with correlation coefficient greater than 0.99. Wind load level was designated twofold: direct mapping of fluid dynamic analysis and conversion of modeled results into wind pressure coefficients (C_P). Finally, design criteria of EN1991-1-4 and NEN3859 were applied in terms of their wind pressure coefficients for comparison. C_P of CFD result was low in the most of the modeled area but was high only in the first roof wind facing and the last lee facing areas. Besides, structural analysis results were similar in terms of stress distribution as per EN and direct mapping while NEN revealed higher level of stress for the last roof area. The maximum stress levels are arranged in decreasing order of mapping, EN, and NEN, generating 8% error observed between the EN and mapping results under 30 m/sec of wind velocity. On the other hand, effect of dead weight on the stress distribution was investigated via variation of high stress position with wind velocity, confirming shift of such position from the center to the forward head wind direction. The sensitivity of stress for wind velocity was less than 0.8% and negligible at wind velocity greater than 20 m/sec, thus eliminating self-weight effect.

Keywords: computational fluid dynamics (CFD); stress distribution; venlo-type greenhouse; wind load; wind pipe; Wind pressure coefficients (C_P)

1. Introduction

Recently, horticultural facility has significantly improved and increased in numbers, thus enabling to maintain the most suitable environment for cultivation of crops and the ensuing market competitiveness of the harvested crops. Typically, greenhouse consists of massive superstructure with lightweight nature. However, such greenhouse structure is designed to withstand sudden and violent climate change caused by global warming, such as heavy snow and rainfall and a gale and gusty wind. The mainstream of the most desirable greenhouse structure is centered around pursuit of lighter weight. Vieira Neto *et al.* (2016) studied stress distribution of the greenhouse structure in terms of wind load as per EU and Brazilian standards. Park *et al.* (2005) also investigated stress distribution analysis caused by wind load using optimized design method. On the other hand, natural ventilation characteristics was suggested by Khaoua *et al.* (2006) via computational fluid dynamics(CFD) analysis performed on the outside wind direction and the effect of the ventilation window. The pressure coefficients distribution for various low-rise buildings including greenhouse is predicted by CFD simulation and experiments (Kateris *et al.* 2012, Kozmar 2011, Lopes *et al.* 2015, Shklyar and Arbel 2004). Cao *et al.* (2010) have used the arbitrary Lagrangian–Eulerian approach to analyze structural safety of a flexible container roof for strong wind loads. Guand Huang (2015) studied the equivalent static wind load of large span roof structures. Moriyama *et al.* (2015) simultaneously performed wind tunnel experiment and CFD to correlate shape of the single vinyl greenhouse unit and the pattern of its multiple arrangement and the significant factors affecting pressure indices therefrom. Similar research was also performed by Kwon *et al.* (2016), evaluating wind pressure coefficients for a single vinyl greenhouse unit of various geometries based on wind tunnel experiment simulating air streams prevalent in the coastal reclaimed land. Last category on such studies is represented by Brookhorst *et al.* (2017) who studied wind load analysis for stability of the massive multi-span duo-pith greenhouse. Lastly, Nayak *et al.* (2014) investigated into the wind load analysis on the greenhouse with emphasis on structural stability. The aforementioned literature results rather comprehensively reflect the pressure coefficients for various parameters such as geometry and span number of the greenhouse via experiment and analytical methods or used a simple beam model for evaluation of the structural safety based on the calculated bending moment and stress

*Corresponding author, Ph.D.
E-mail: djhur@iae.re.kr
[a] Ph.D.
E-mail: junghunnoh@iae.re.kr
[b] Master
E-mail: leehj@iae.re.kr
[c] Ph.D.
E-mail: hwsong@iae.re.kr

http://www.techno-press.com/journals/was&subpage=7
ISSN: 1226-6116 (Print), 1598-6225 (Online)

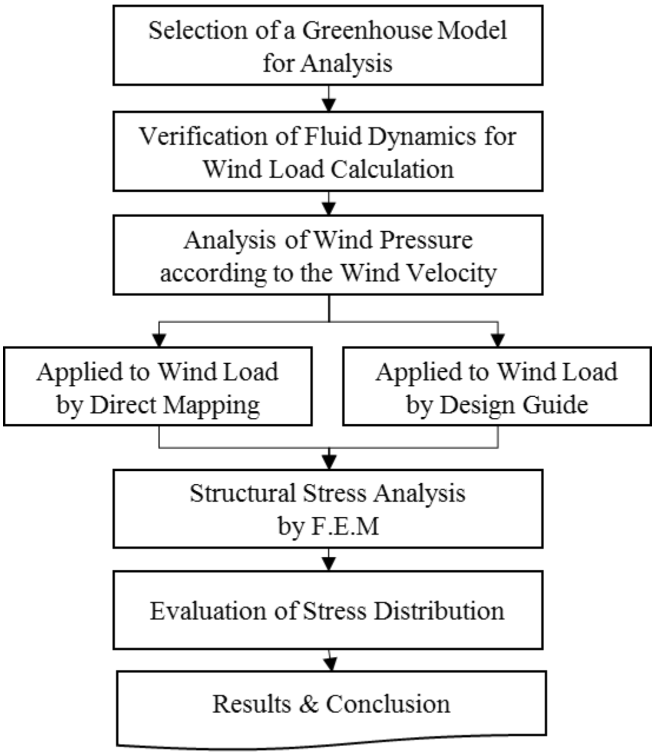

Fig. 1 Flowchart of numerical analysis

of the main post.

A dearth of literature is found in the area of precise modeling for structural analysis as affected by various stress sources such as wind (velocity) and gravity with eventual objective of securing structural safety. In the present paper, complex stress state caused by combination of dead load and wind load was modeled via CFD to examine its effect on the variation of stress distribution in the (greenhouse) structure. Modeling result was cross-checked for enhanced reliability by experiment based on single greenhouse unit example. Two methods are employed for wind load modeling for analysis of stress distribution: direct mapping method using the pressure obtained by the CFD analysis on the wind to the contact area of the greenhouse and the ensuing interpretation using the wind load factor reflected in the design. Fig. 1 shows flowchart for CFD analysis.

2. Numerical analysis method

2.1 Theoretical considerations

2.1.1 Fluid dynamics

The theoretical review consists of two parts: fluid dynamics and structural analysis. The governing equations for fluid dynamics modeling are described in (2) through (5)

Mass conservation equation

$$\frac{\partial \rho}{\partial t} + \nabla \cdot \left(\rho \vec{u}\right) = 0 \qquad (2)$$

Momentum conservation equation

$$\frac{\partial\left(\rho \vec{u}\right)}{\partial t} + \nabla \cdot \left(\rho \vec{u}\vec{u}\right) = -\nabla P + \nabla \cdot \left(\mu \nabla \vec{\mu}\right) \qquad (3)$$

Transport equation for kinetic energy (κ) (standard κ-ε model)

$$\frac{\partial(\rho\kappa)}{\partial t} + \nabla \cdot \left(\rho\kappa\vec{u}\right) = \nabla \cdot \left[\left(\mu + \frac{\mu_t}{\sigma_\kappa}\right)\nabla\kappa\right] + G_\kappa + G_b - \rho\varepsilon - Y_M \qquad (4)$$

Transport equation for ε (standard κ-ε model)

$$\frac{\partial(\rho\varepsilon)}{\partial t} + \nabla \cdot \left(\rho\varepsilon\vec{u}\right) = \nabla \cdot \left[\left(\mu + \frac{\mu_t}{\sigma_\kappa}\right)\nabla\varepsilon\right] + \rho C_2 \frac{\varepsilon^2}{\kappa + \sqrt{\nu\varepsilon}} + C_{1s}\frac{\varepsilon}{\kappa}C_{3s}G_b \qquad (5)$$

The coefficients in Eq. (5) are assigned standard values

C_2 = 1.92, C_{1s} = 1.44, C_{3s} = 0.33.

Here, the parameters are also listed as follows:

$\vec{u}$: velocity vector;
P : static pressure:
t : time;
κ : turbulence kinetic energy;
ε : rate of dissipation for;
μ : dynamic viscosity;
μ_t : turbulent viscosity
σ_κ : turbulent Prandtl numbers for κ .

In Eq. (4), G_κ , G_b , Y_M represent generation of turbulence kinetic energy due to the mean velocity gradients, generation of turbulence kinetic energy due to buoyancy and is the contribution of the fluctuating dilatation in compressible turbulence to the overall dissipation rate, respectively (Launder *et al.*1974). The mass and momentum equations were solved for the flow analysis, and the standard κ-ε modeling was also performed to reflect turbulence modeling analysis with high Reynolds number. Air temperature, its density and viscosity for the flow field modeling were taken as 20℃, 1.207 kg/m^3 and 1.85 × 10^{-5}kg/m-s, respectively. Boundary condition of the analytical modeling consists of velocity inlet and pressure outlet for entrance and the outlet, respectively while non-slip conditions were applied to the bottom area. Inlet velocity varies with height, necessitating the wind speed variation with the roughness of the ground surface. The velocity profileand turbulence intensity measured by Kwon *et al*. (2016) was applied to the numerical model.

2.1.2 Static structural analysis

The equilibrium relations for a statically modeled body (Sokolnikoff 1956) are derived from the following Eqs. (6) to (9). Using the static equilibrium relation of between the forces and deformation,

$$\sigma_{ij,j} + f_i = \rho \ddot{w}_i \tag{6}$$

where $\sigma_{ij,j}$, f_i, and $\ddot{w}_i$ are stress tensor, body force, and the resulting acceleration.

On the other hand, stress-strain equations and compatibility equations are given as (7) and (8)

$$\sigma_{ij} = c_{ij,kl} \cdot \varepsilon'_{kl} \tag{7}$$

where $c_{ij,kl}$and ε'_{kl} represent stiffness constant and strain, respectively.

For any arbitrary displacement field $w(x_1, x_2, x_3)$, strains is directly computed from the strain-displacement equation.

$$\varepsilon'_{kl} = \frac{1}{2}(w_{i,j} + w_{j,i}) \tag{8}$$

Stress is then calculated using a finite element method with discrete element-wise modeling of structural geometry with specific boundary conditions and material data.

Two methods were used to input wind load, i.e., direct mapping of the CFD analysis results and by application of wind pressure coefficient. The latter procedure is further explained by Eq. (9)

$$L_w = c_p \cdot v^2 \tag{9}$$

where L_p, c_p and v are wind load, pressure coefficient, and wind speed, respectively.

2.2 Analytical modeling

2.2.1 Verified model of fluid results (pressure coefficient)

The subject of this study is a Venlo-type Greenhouse, as shown in Fig. 2. The Numerical Analysis model also uses a reduced model for comparison with the test results by Kwon *et al*. (2016). The simplified model closely simulated the actual model, both geometrically and kinematically. Therefore, the geometric and kinematic similarity ratios were taken as 1:20 and 1:6, respectively.

Fig. 2 show schematic diagram of the numerical analysis domain and the whole domain of the numerical analysis model, respectively. Fig. 2(b) shows detailed shape of the greenhouse with the precise dimensions listed in Table 1.

The grid resolution was set to be 2.62 million along x-, y- and z-directions. Fine grids were used near the wall of greenhouse, and the size of the grid cell at the wall was about 10 mm. Grid independence of the solution was checked with finer grids up to 3.78 million along x-, y- and z-directions. The difference in maximum pressure coefficient (C_P) of greenhouse wall between the reference grid system and finer grid system was less than 1 %.

An experimental study was conducted based on the theory of wind characteristics with ESDU 8411 and 8430 (ESDU. 2005) for the Venlo type greenhouse (Kwon *et al*. 2016). Therefore, in this study, the average velocity distribution according to the inlet height is as follows.

$$u = 0.186 \cdot log(100 \cdot h) + 2.39 \tag{10}$$

where u and h represent the inlet velocity at some point of concern and the height of fluid domain, respectively. Here, the turbulence intensity was applied to the numerical model with the average value (16%), that is 15~20% depending on the height of the inlet.

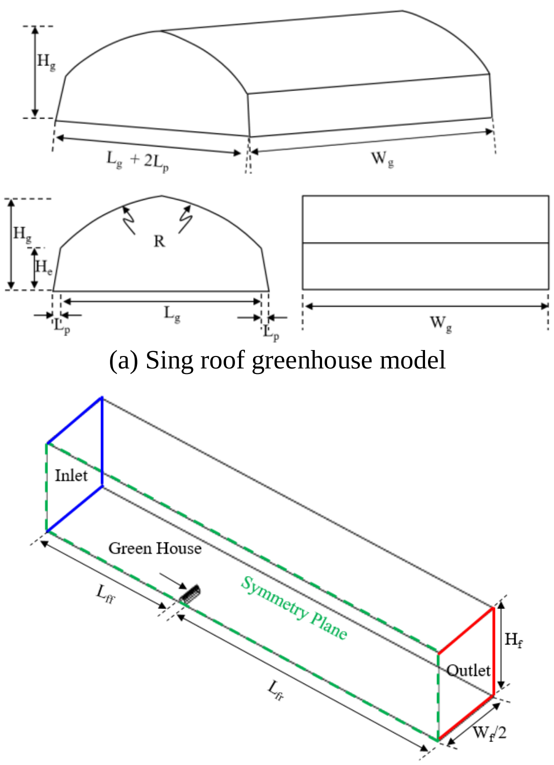

Fig. 2 Schematic modeling dimension for fluid analysis verification. Detailed dimension is available in Table 1

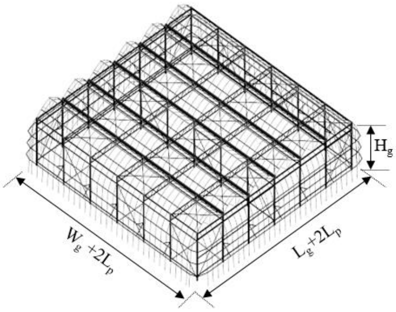

(a) Isometric view

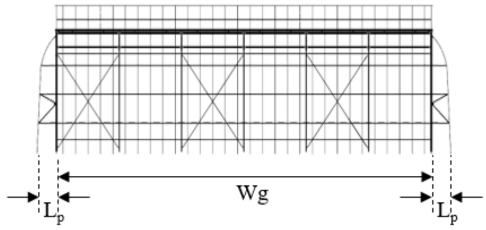

(b) Front view

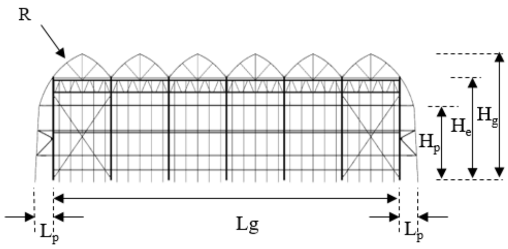

(c) Side view

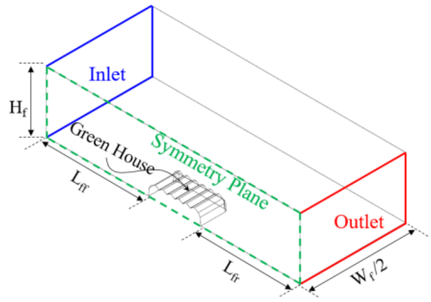

(d) Isometric view of fluid filed for the modeled wind pressure

Fig. 3 Schematic modeling dimensions for fluid and structural analyses. Detailed dimension is available in Table 1

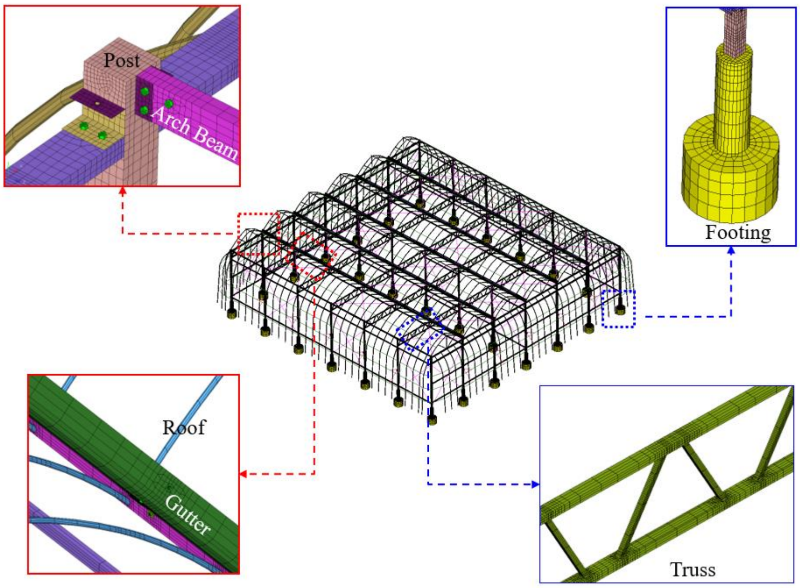

Fig. 4 Finite element modeling of the base line design for the greenhouse structure

The wind pressure coefficient represents the force acting along the surface of the greenhouse caused by fluid flow on the surface of the greenhouse. The wind pressure coefficient is described as follows.

$$C_p = \frac{p - p_0}{\frac{1}{2}\rho U^2} \tag{11}$$

where C_p, p, p_0, ρ, U has their respective usual significance of an average wind pressure coefficient at some point of concern, static pressure, static pressure of the undisturbed stream, density of the air and velocity of the undisturbed stream.

Table 1 Dimensions for the fluid and structural analyses modeling of the greenhouse (unit: m)

	Symbol description	Multi-roof	Single-roof
H_f	Height of fluid domain	60.0	2.5
W_f	Width of fluid domain	310.0	8.0
L_{ff}	Front Length of fluid domain	99.7	7.83
L_{fr}	Rear Length of fluid domain	99.7	15.0
H_g	Height of greenhouse	6.3	0.175
H_e	Height of eave	5.1	0.08
H_p	Height of straight wind pipe	3.7	-
H_g	Length of greenhouse	23.2	0.33
L_p	Length of wind pipe	1.2	0.01
W_g	Width of green house	24.1	1.1
R	Radius of roof curvature	4.0	3.0

Table 2 Materials properties of the greenhouse structure

Part	Materials	Density (kg/m^3)	Elastic modulus (MPa)	Poisson's ratio
Frame	SS400	7.85E-6	200,000	0.3
Al- Frame	Aluminum	2.7E-6	69,000	0.33
Footing	Concrete	2.4E-6	28,600	0.15

2.2.2 3-Span model for fluid and structural analyses

The modeled greenhouse structure is of a 3-span arch type as depicted in Fig. 3, where 560 m^2 of floor area are illustrated. Dimension of the flow field domain for the fluid dynamics modeling analysis is also detailed in Fig. 3 and Table 1. Fluid dynamic modeling space is designed to minimize boundary area effect and thus more than 8 times of the actual greenhouse length and height and 4times of its width were taken to account for the entire modeling space as schematically detailed in Fig. 3(d). Structural modeling consists of finite element method analysis as shown in Fig. 4 with combination of 1-, 2-, and 3-dimensions. Boundary condition was set by the rigid interface between the greenhouse and the ground. Relevant materials properties for the structure are available in Table 2. To investigate into the effect of wind load on the greenhouse structure, dual methods of direct mapping of the fluid dynamic analysis results into the nodes of the structural model as well as calculation of the wind load by calculation via wind pressure coefficients given by design guide were used.

3. Result and discussion

For reliability analysis of fluid dynamics modeling, results for a peach-type greenhouse are represented for calculation of average wind pressure coefficient with variation of rooftop surface angular segments and compared with experimental results by Kwon *et al.* (2016). Such results are compared by normalized wind pressure coefficient, which is schematically shown in Fig. 5: correlation coefficient of 0.99 represents reasonably good agreement between the modeling and experiment: positive pressure generated at the windward surface and negative pressure developed at the leeward surface, consistent with both of the modeling and experimental results. Negative pressure increased from ledge to ridge on a windward surface while it decreased from ridge to ledge on the leeward surface. For R05~R08 of Fig. 5, wind pressure decreased on the leeward surface from ridge to ledge, which is attributed to breakaway of the turbulent flow and such phenomenon is commonly observed in both modeling and experiment. 3-span greenhouse was similarly simulated for fluid dynamic modeling analysis and Fig. 6 shows distribution of wind pressure and wind velocity.

Fluid dynamic characteristics depicted in Fig. 6 shows head wind to the forward surface area where a positive pressure is applied and the other area subject to negative pressure caused by increased wind velocity. Such behavior is quite similar to what is represented by a single unit greenhouse. Maximum wind velocity is observed at the upper tip of the first roof and the wind pressure coefficient of the first roof is expected to be the highest. Wind load distribution along the overall surface of the greenhouse is also modeled for variation of the basic wind speed between 6~30 m/sec, which is converted to wind pressure coefficients and listed in Table 3. Use of wind pressure coefficient as a design guide for a greenhouse is thus justified regardless of the wind velocity in view of the minimal correlation between the wind velocity and wind pressure coefficients.

Design criteria of the greenhouse were evaluated in Table 4 based on CFD modeling, especially related to wind pressure coefficients. The CFD modeling results of Table 4 closely approach EU standard of EN1991-1-4.

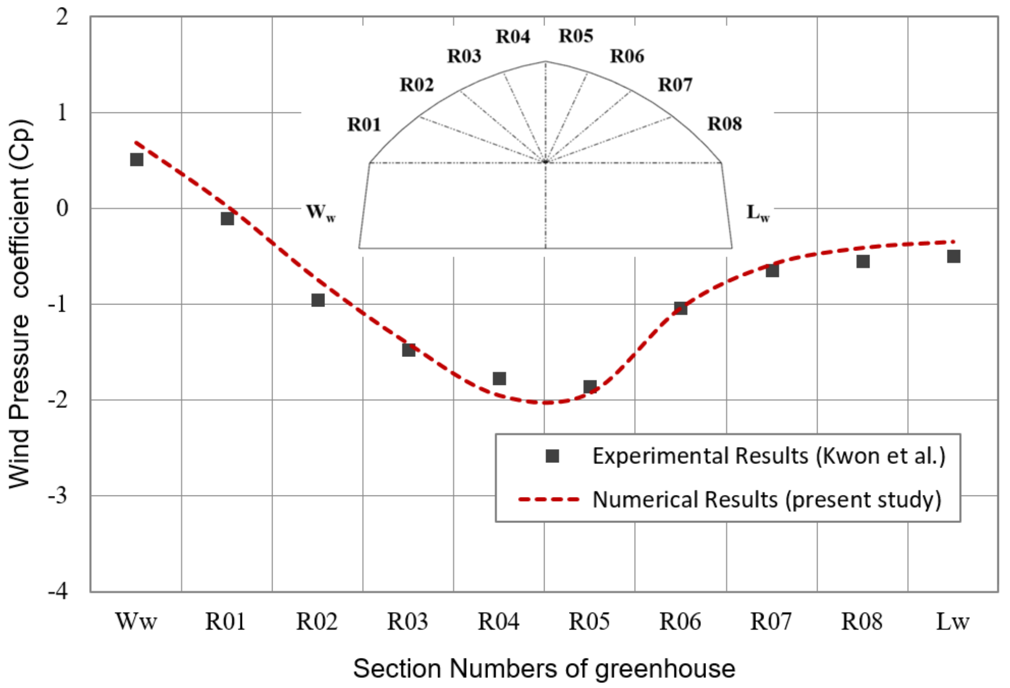

Fig. 5 A Comparison between modeling and experiment for wind pressure coefficient of a single peach-type greenhouse roof (correlation coefficient = 0.99)

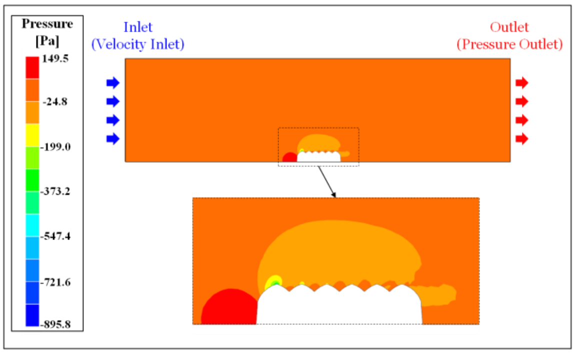

(a) Pressure contour

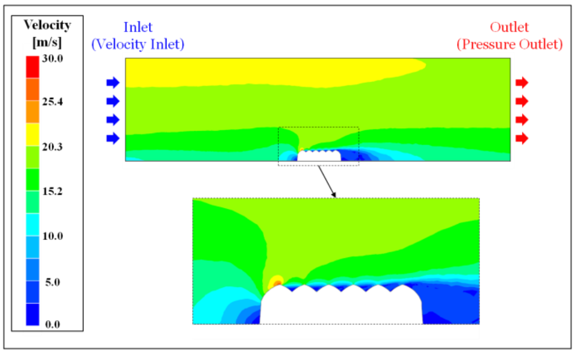

(b)Velocity contour

18.0 m/sec

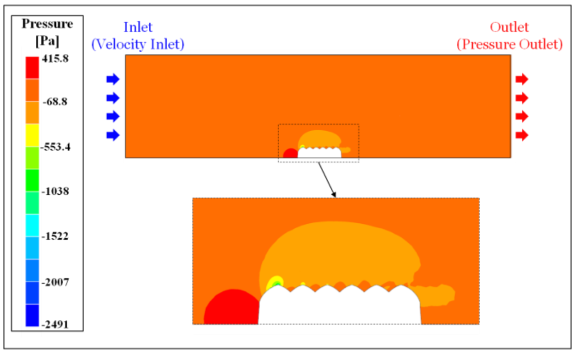

(a) Pressure contour

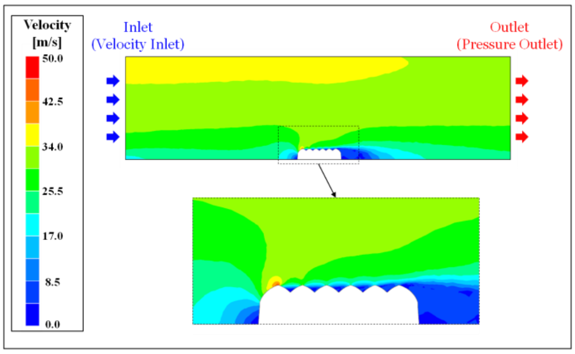

(b)Velocity contour

30.0 m/sec

Fig. 6 Distribution of the pressure caused by wind load and the velocity of the peach-type multi- roof greenhouse

Table 3 Variation of wind load pressure coefficients with velocity (wind speed unit: m/sec)

W	Roof face												Front face	Rear face	Side face
	A	B	C	D	E	F	G	H	I	J	K	L	M	N	O
6	-0.88	-1.06	-0.72	-0.46	-0.31	-0.33	-0.20	-0.30	-0.17	-0.33	-0.21	-0.5	0.79	-0.3	-0.41
12	-0.88	-1.06	-0.72	-0.46	-0.31	-0.33	-0.20	-0.30	-0.17	-0.33	-0.21	-0.5	0.79	-0.29	-0.41
24	-0.88	-1.06	-0.72	-0.46	-0.31	-0.33	-0.20	-0.30	-0.17	-0.32	-0.21	-0.5	0.80	-0.29	-0.41
30	-0.88	-1.06	-0.72	-0.46	-0.31	-0.33	-0.20	-0.30	-0.17	-0.32	-0.21	-0.5	0.80	-0.29	-0.41

W: Wind speed

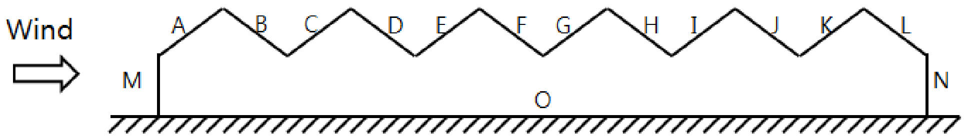

Table 4 Comparison between CFD modeling results and corresponding EU and Korean standards for greenhouse design in terms of wind pressure coefficients

	Roof face												Front face	Rear face	Side face
	A	B	C	D	E	F	G	H	I	J	K	L	M	N	O
EN	-1.1	-1.0	-0.7	-0.5	-0.4	-0.5	-0.4	-0.4	-0.4	-0.4	-0.4	-0.4	0.6	-0.6	-0.4
NEN	-0.6	-1.0	-0.7	-0.5	-0.4	-0.5	-0.4	-0.4	-0.4	-0.4	-0.4	-0.4	0.6	-0.3	-0.3
CFD1	-0.9	-1.1	-0.7	-0.5	-0.3	-0.4	-0.2	-0.3	-0.2	-0.4	-0.2	-0.5	0.8	-0.3	-0.4
CFD2	-1.4	-1.0	-0.4	-0.5	-0.2	-0.4	-0.2	-0.4	-0.2	-0.4	-0.3	-0.9	0.7	-0.3	-0.4

EN: EN1991-1-4, NEN: NEN3859, CFD: Computational fluid Dynamic
CFD1 : Pitch-type roof, CFD2 : Arch-type roof

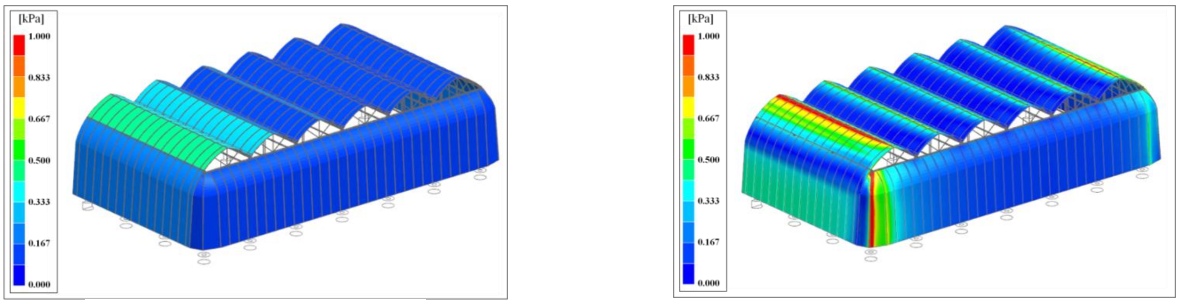

(a) Wind load with EN1991-1-4 (b) Wind load with direct mapping

Fig. 7 Variation of wind pressure distribution for different wind load application methods

However, it is also to be stressed that the CFD results of the head wind to the first roof and the lee-facing final roof have been underestimated. On the other hand, more than 10% of safety factor has been obtained for other greenhouse roof faces. Lastly, front roof shows higher wind pressure coefficients for arch type greenhouse unit compared to peach type unit.

Next structural analysis consists of response of the greenhouse unit with variation of the wind load. As previously mentioned, wind loads were applied in two ways: wind pressure as obtained from the CFD modeling was directly mapped or conversion equation for wind pressure coefficients of Eq. (9) was used. Distribution of wind pressure over the greenhouse roof is shown in Fig. 7 for both cases and overall contour is quite similar with noticeable local discrepancy. More specifically, wind pressure distribution varied within the same roof surface via direct mapping and resultant load path variation is also expected, thus affecting local stress distribution.

Fig. 8 shows variation of stress with wind velocity and wind load application methods: stress was concentrated at the truss for low wind pressure but forward arch is subject to concentrated stress with increased wind velocity. EN1991-1-4 and CFD modeling dictate high stress at the rear surface at wind velocity of 30 m/sec but this aspect is not dictated by NEN3895 criterion. Therefore, CFD analysis results are more comprehensively justified by EN1991-1-4 than NEN3895 standard.

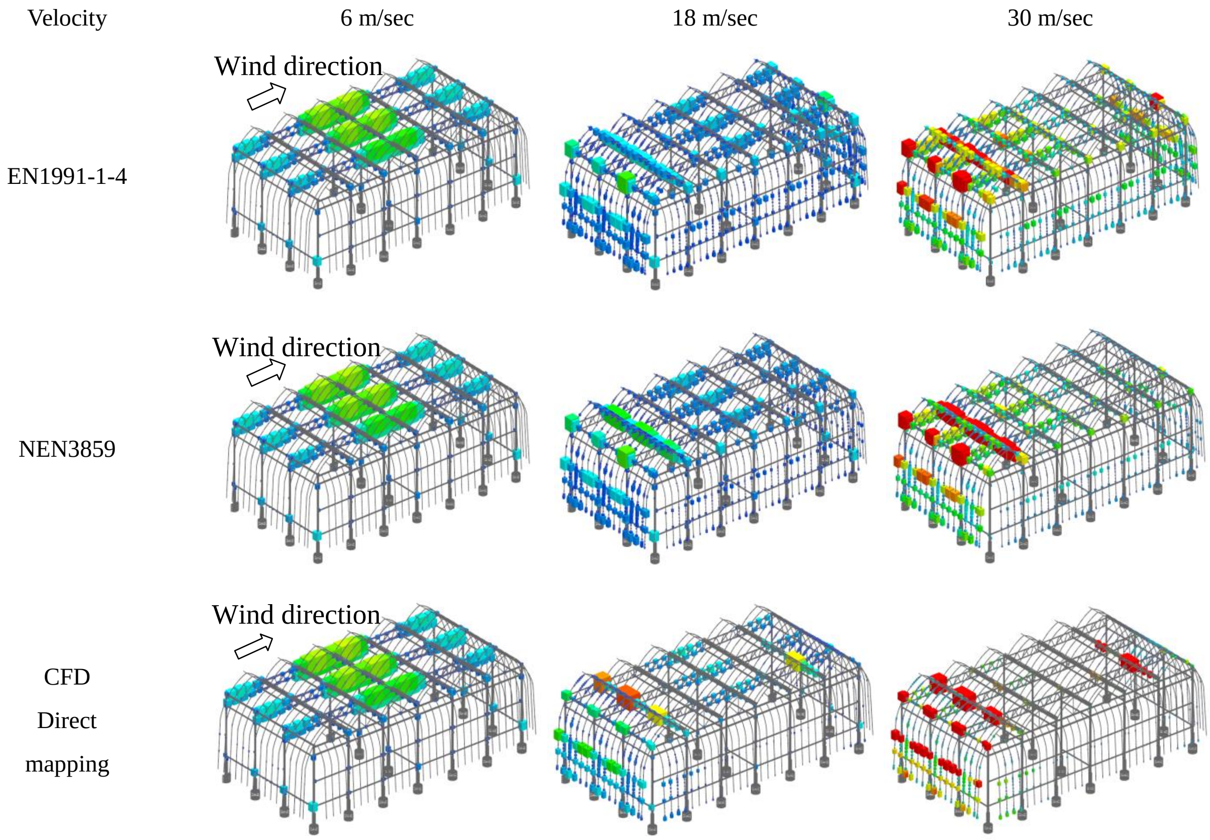

Fig. 8 Stress distribution contour for variation of wind velocity and relevant standards as compared with CFD modeling under common wind load and gravity condition

Table 5 Maximum stress levels with variation of wind velocity for different wind load input methods under simultaneous effect of gravity (unit: MPa)

	0 m/sec	6 m/sec		12 m/sec		18 m/sec		24 m/sec		30 m/sec	
	G	W	W+G	W	W+G	W	W+G	W	W+G	W	W+G
EN1991-1-4	85.9	14.4	80.7	57.7	65.1	129.8	120.0	230.8	221.0	360.6	350.7
NEN3859	85.9	13.7	80.8	54.7	65.6	123.1	113.4	218.8	209.1	342.0	332.2
CFD Direct mapping	85.9	15.4	81.9	62.0	69.7	139.7	125.8	248.6	231.2	388.8	366.8

G : gravity load, W : wind load, G+W : gravity load + wind load

Variation of maximum wind load with wind velocity was subsequently investigated for structural safety evaluation as detailed in Table 5. The maximum wind loads in Table 5 are listed in the decreasing order as obtained by CFD modeling via direct mapping, EN1991-1-4, and NEN3858. Therefore, maximum wind stress was lower for CFD modeling via direct mapping and this is attributed to reflection of local stress variation with ensuing possibility of safety evaluation, thus generating more accurate analysis compared to EN and NEN standards where only average pressure distribution is considered. One thing is also noteworthy in that simultaneous application of gravity and wind load caused lower stress and this is attributed to direction-wise counter-action of gravity and wind load. On the other hand, gravity-induced stress constituted more than 20% for wind velocity of 30 m/sec but maximum stressed spot experienced stress level of 22 MPa, which is less than 5.7% of allowed stress level.

For overall representation of stress distribution, stress variation with wind velocity is also graphically examined for selected stress concentration areas in Fig. 9.

Fig. 9 shows non-linear variation of stress with velocity, proportional to square of velocity: truss area showed somewhat peculiar stress variation of inverse proportionality to velocity and normal proportionality relation. This is caused by counter-directionality of the gravity and wind load. To elucidate the effect of gravity further, stress variation rate with wind velocity is detailed in Fig. 10, where the rate of change approaches constant asymptotic value with linear relation (less than 0.8% error)

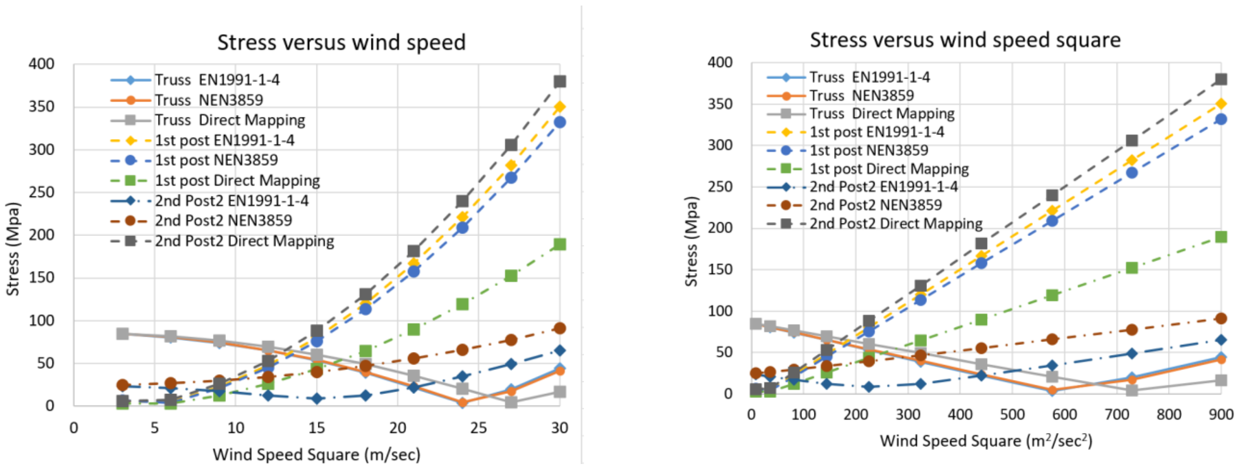

(a) Stress versus wind speed (b) Stress versus wind speed square

Fig. 9 Stress variation with wind speed for selected stress concentration areas

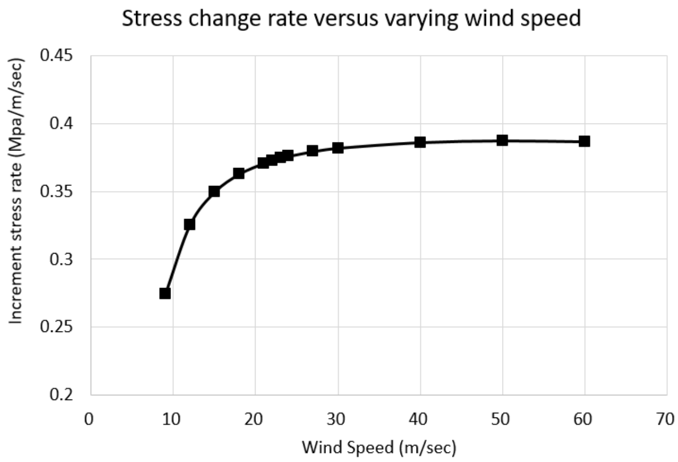

Fig. 10 Stress variation rate with wind speed

obeyed at 20 m/sec with reference to 30 m/sec. This is attributed to decreased effect of stress with velocity. Therefore, the effect of gravity should be taken into consideration at low wind velocity.

4. Conclusions

In the present paper, parameters affecting structural stability of a Venlo-type greenhouse unit were investigated using fluid dynamic and structural analyses based on wind tunnel test results. For reliability analysis, fluid dynamic analysis modeling results were compared with experiment, corroborating credibility of applied modeling approach within R = 0.99 of correlation coefficient. As for pressure coefficients analysis results, EN1991-1-4 criterion more closely simulated and NEN3895 criterion is rather underestimated. Pressure coefficient of arch type greenhouse showed larger pressure coefficient of front roof while NEN3895 criterion rather underestimated such aspect. More specifically, arch type greenhouse showed larger pressure coefficient of front roof than peach-type greenhouse. Stress distribution of greenhouse structure varied with method of applying wind load and simultaneous application of wind load and gravity resulted in lower than their individual effect caused by their counter-directionality. Increased wind velocity also caused shifting of maximum stress concentration area from truss to roof arch under simultaneous application of gravity. In view of this, truss area should be strengthened under lower wind velocity condition and roof arch should be strengthened under high wind velocity condition. Design criteria underestimated levels of stress at some local areas compared to direct mapping, which is attributed to different values of applied stress levels: individual stress levels are applied during mapping while average stress levels are applied in the design criteria, causing pressure differentials within roof surface and resulting in local stress in the roof arch material. Lastly, stress is linearly proportional to square of wind velocity but non-linear relation was observed at low wind velocity under simultaneous application of gravity. However, sensitivity of stress for wind velocity was negligible to less than 0.8% above certain wind velocity of 20 m/sec.

Acknowledgments

This research was supported by Export Promotion Technology Development Program (Project No. 114083-03), Ministry of Agriculture, Food and Rural Affairs.

References

Bronkhorst, A.J., Geurts, C.P.W., van Bentum, C.A., van der Knaap, L.P.M. and Pertermann, I. (2017), "Wind loads for stability design of large multi-span duo-pitch greenhouses. front", *Built Environ*., **3**(18), 13031-1.

Cao, Y., Wang, P. and Jin, X. (2010), "Dynamic analysis of flexible container under wind actions by ALEfinite-element method", *J. Wind Eng. Ind. Aerod*., **98**(12), 881-887.

ESDU. (2005), Computer program for wind speeds and turbulence properties: flat or hilly sites in terrain with roughness changes. Engineering Science Data Unit. ESDU Data Item: 01008

Gu, M. and Huang, Y. (2015), "Equivalent static wind loads for stability design of large span roof structures", *Wind Struct*., **20**(1), 95-115.

Kateris, D.L., Fragos, V.P., Kotsopoulos, T.A., Martzopoulou, A. G. and Moshou, D. (2012), "Calculated external pressure coefficients on livestock buildings and comparison with Eurocode 1", *Wind Struct*., **15**(6), 481-494.

Khaoua, S.O., Bournet, P.E., Migeon, C., Boulard, T. and Chassériaux, G. (2006), "Analysis of greenhouse ventilation efficiency based on computational fluid dynamics", *Biosyst. Eng*., **95**(1), 83-98.

Kim, K., Yoon, J.Y., Kwon, H.J., Han, J.H., Son, J.E., Nam, S.W., Giacomelli, G.A. and Lee, I.B. (2008), "3-D CFD analysis of relative humidity distribution in greenhouse with a fog cooling system and refrigerative dehumidifiers", *Biosyst. Eng*., **100**(2), 245-255.

Kim, R.W. (2015), "Evaluation of Wind Pressure Coefficients of Greenhouses using Wind Tunnel Test and Numerical Model", Doctoral dissertation, Seoul National University, Seoul, Korea

Kozmar, H. (2011), "Wind-tunnel simulations of the suburban ABL and comparison with internationalstandards", *Wind Struct*., **14**(1), 15-34.

Kwon, K.S., Kim, D.W., Kim, R.W., Ha, T. and Lee, I.B. (2016), "Evaluation of wind pressure coefficients of single-span greenhouses built on reclaimed coastal land using a large-sized wind tunnel", *Biosyst. Eng*., **141**, 58-81.

Launder, B.E. and Spalding, D.B. (1974), "The numerical computation of turbulent flows", *Comput. Method. Appl. M*., **3**(2), 269-289.

Li, L., Kareem, A., Hunt, J., Xiao, Y., Zhou, C. and Song, L. (2015), "Turbulence spectra for boundary-layer winds in tropical cyclones: a conceptual framework and field measurements at coastlines", *Bound.-Lay. Meteorol*., **154**(2), 243-263.

Lopes, M.F.P., Paixão Conde, J.M., Glória Gomes, M. and Ferreira, J.G. (2010), "Numerical calculation of thewind action on buildings using Eurocode 1 atmospheric boundary layer velocity profiles", *Wind Struct*., **13**(6),487-498.

Moriyama, H., Sase, S., Okushima, L. and Ishii, M. (2015), "Which design constraints apply to a pipe-framed greenhouse?", *Japan Agricultural Research Quarterly: JARQ*, **49**(1), 1-9.

Nayak, A.K. and Rao, K.R. (2014), "Estimation of wind load on a greenhouse and evaluation of its structural stability", *Int. J. Agricultural Eng*., **7**(2), 461-466.

Park, C.W., Lee, J.W., Lee, H.W. and Lee, S.G. (2005), "Optimum design of greenhouse structures using continuous and discrete optimum algorithms", *J. Korean Association for Spatial Structures*, **5**(4), 61-70.

Park, C.W., Yuh, B.Y., Lee, H.W. and Lee, S.G. (2007), "Optimum design of greenhouse structures using genetic algorithms", *J. Korean Society of Steel Construction*, **19**(2), 171-179.

Shademan, M., Barron, R.M., Balachandar, R. and Hangan, H. (2014), "Numerical simulation of wind loading on ground-mounted solar panels at different flow configurations", *Can. J. Civil Eng*., **41**(8), 728-738.

Shklyar, A. and Arbel, A. (2004), "Numerical model of the three-dimensional isothermal flow patterns and mass fluxes in a pitched-roof greenhouse", *J. Wind Eng. Ind. Aerod*., **92**(12), 1039-1059.

Sokolnikoff, I.S. (1956), Mathematical Theory of Elasticity, McGraw-Hill Book Co, New York, NY, USA.

Vieira Neto, J.G. and Soriano, J. (2016), "Distribution of stress in greenhouses frames estimated by aerodynamic coefficients of Brazilian and European standards", *Scientia Agricola*, **73**(2), 97-102.

AD